Numerical Simulation on the Ventilated Cavitating Flow with High Froude Number

M. Xiang[1,2*], H.W. Zhang[1] and J.Y. Tu[2,3]
[1]Institute of Aerospace and Material Engineering, National University of Defense Technology, Changsha 410073, P.R. China
[2]Institute of Nuclear and New Energy Technology, Tsinghua University Beijing 100084, China
[3]School of Aerospace, Mechanical and Manufacturing Engineering RMIT University, Victoria 3083, Australia
e-mail: jiyuan.tu@rmit.edu.au

Received: 10 October 2012, Accepted: 30 April 2013

Abstract
A numerical scheme based on the homogeneous multiphase model was proposed to model the ventilated cavitating flow by considering interaction between three phases including vapor, ventilated gas and liquid. Due to the difficulty of carrying out ventilated cavitation experiments in high-speed water tunnels, focus was put on predicting the developing process of the cavitating flow with high Froude number. The evolution processes for the ventilated cavity which transited between different gas-leakage mechanisms were successfully captured, obtaining the variation of the cavitation number along with the ventilation rate. Hydrodynamics analysis was carried out for the cavitating body with low and high Froude number respectively, thereby revealing the ventilation rate to optimize the vehicle performance. Based on the numerical results, a theoretical gas-leakage model which was adapted to a wide range of Froude number and various gas-leakage mechanisms was proposed. The model was validated through comparison against experimental data and numerical results. This research provides valuable guidance on the design for ventilated cavitating vehicles.

Keyword: Ventilated cavitation; Gas-leakage; Hydrodynamics; Numerical simulation.

1. INTRODUCTION

For high speed fully-submerged underwater vehicles, e.g. projectiles and torpedoes, ventilated cavitation [1–4] has been proposed to realize drag reduction by injecting gas in the wake region behind a cavitator, forming a continuous cavity covering the object surface. With the entire body being immersed in the cavity, friction drag can be significantly reduced by over 90% [5].

In the past decades, numerous research has been carried out to better understand the formation mechanism [6, 7] for the ventilated cavity. It was found out that the evolution process of the ventilated cavity was not only related to the ventilation condition but also related to the gas-leakage schemes [8, 9] which was strongly governed by two important parameters: cavitaion number σ_c and Froude number Fr. When magnitudes of the numbers Fr and σ_c are high, the gravity effect is ignorable and the cavity shape is close to the axisymmetric one. The continuous ventilated cavity is broken down by the re-entrained jet at the cavity tail where the gas pockets are lost in the form of toroidal vortices; When numbers Fr and σ_c are small and the gravity effect dominates, the cavity ends by two hollow vortex tubes carrying over the gas from the cavity. Great efforts have been put forward on establishing the theoretical models to calculated the complex cavity shape under different working conditions based on the experimental results. Cox and Clayden [9] established the empirical gas-leakage model for the ventilated cavity with twin-vortex tubes, which was only

*Corresponding author. Tel.: +86-731-84576482; fax: +86-731-845731235. Email: xiangmin333@hotmail.com

adaptive for the low Froude number condition. Campbell and Hiborne [8] further improve the model by considering the cavitator diameter. Spurk [10] has established the gas loss model for re-entrained jet mechanism using boundary layer theory. However, as the freestream velocity is limited to motor power, most of the experiments were carried out in the low speed water tunnel, which gave rise to low Froude number. To date, none of the universal model is developed to calculate the cavity shape with high Froude number. Considering that the ventilated cavitating vehicles are usually required to work at high speed to achieve long voyage, the development of the ventilated cavity with high Froude number needs to be further understood in order to better control the cavitating vehicles.

In this paper, a numerical model which is capable of predicting the interaction between vapor, ventilated gas and liquid for the ventilated cavitating flow is established based on the homogeneous multiphase model. The experiments carried out at St. Anthony Falls Laboratory of the University of Minnesota [11] are used to validate the numerical model. Particular emphasis is then directed towards a better understanding on the formation mechanisms for the ventilated cavity with high Froude number. Hydrodynamics analysis including drag and lift coefficient for the cavitating body is carried out to optimize the design of the cavitating vehicle. A theoretical model for calculating the cavity shape with various gas-leakage mechanisms and wide Froude number is proposed based on the numerical results.

2. MATHEMATICAL MODELS

2.1. Governing Equations

The model is established based on the homogeneous multiphase model where the fluid is assumed to be a mixture of liquid, vapor and non-condensible gas. The components share the same velocity and pressure. As the heat transfer is ignored in this research, the governing equations are described as follows:

The continuity equation for the mixture phase:

$$\frac{\partial(\rho_m)}{\partial t} + \nabla \boldsymbol{g}(\rho_m \boldsymbol{u}) = 0 \tag{1}$$

The momentum equation for the mixture phase:

$$\frac{\partial(\rho_m \boldsymbol{u})}{\partial t} + \nabla \boldsymbol{g}(\rho_m \boldsymbol{u} \otimes \boldsymbol{u}^T) = -\nabla p + \nabla \boldsymbol{g}\left[(\mu_{l,l} + \mu_{t,m})(\nabla \boldsymbol{u} + \nabla \boldsymbol{u}^T)\right] + \rho_m \boldsymbol{g} + \boldsymbol{F}_s \tag{2}$$

The continuity equation for the vapor phase:

$$\frac{\partial(\rho_v \alpha_v)}{\partial t} + \nabla \boldsymbol{g}(\rho_v \alpha_v \boldsymbol{u}) = \dot{m}^+ - \dot{m}^- \tag{3}$$

The continuity equation for the ventilated non-condensible gas:

$$\frac{\partial(\rho_g \alpha_g)}{\partial t} + \nabla \boldsymbol{g}(\rho_g \alpha_g \boldsymbol{u}) = 0 \tag{4}$$

where $\boldsymbol{u}$ and p refer to the velocity and pressure for the mixture flow. μ_l and μ_t is the molecular and turbulence viscosity. $\boldsymbol{g}$ is the gravity vector, and $\boldsymbol{F}_s$ represents the surface tension force. ρ and α are density and volume fraction respectively. Each subscript of m, v, g, and l represents the mixture phase, vapor, non-condensable gas and liquid, respectively. $\dot{m}^+$ and $\dot{m}^-$ are the source terms induced by evaporation and condensation. The mixture density and laminar viscosity is defined as:

$$\rho_m = \rho_l \alpha_l + \rho_v \alpha_v + \rho_g \alpha_g \tag{5}$$

$$\mu_{l,m} = \mu_{l,l} \alpha_l + \mu_{l,v} \alpha_v + \mu_{l,g} \alpha_g \tag{6}$$

The standard two-equation k~ε model is applied to calculate the mixture turbulence viscosity:

$$\mu_{t,m} = \rho_l C_\mu \frac{k^2}{\varepsilon} \tag{7}$$

where k represents the turbulent kinetic energy and ε describes its dissipation rate. C_μ is a model constant. k and ε are calculated from their transport equations as shown in reference [12]. The conservation equation for the volume fraction is used to close the governing equations:

$$\alpha_l + \alpha_v + \alpha_g = 1 \tag{8}$$

2.2. Cavitation Model

The cavitaiton model is established based on the Rayleigh–Plesset equation [13] where the size of a single vapor/gas bubble is calculated according to the pressure difference between the local static pressure p and the vapor pressure p_v. The cavitation model is described as follows by considering the effect of the ventilated gas [14]:

$$m^+ = C_e \frac{3\rho_v(1-\alpha_v-\alpha_g)\max(\alpha_g,\alpha_{nuc})}{R_\mathrm{B}}\sqrt{\frac{2(p_v-p)}{3\rho_l}}, \quad p < p_v \tag{9}$$

$$m^- = C_c \frac{3\rho_v\alpha_v}{R_\mathrm{B}}\sqrt{\frac{2(p-p_v)}{3\rho_l}}, \quad p > p_v \tag{10}$$

where α_{nuc} is the volume fraction non-condensable gas in liquid, and its value is around $5 \infty 10^{-4}$ for most practical cases. C_e and C_c are the empirical coefcients for different phase change process, and their default values are 50 and 0.01.

2.3. Surface Tension Force

The surface tension force is calculated as continuum surface force [15]:

$$\boldsymbol{F}_s = \sigma\kappa\nabla\alpha_l \tag{11}$$

The curvature κ is calculated using gradients of the interface normal which is calculated using volume fraction gradients:

$$\kappa = -\nabla\cdot\mathbf{n}, \qquad \mathbf{n} = \frac{\nabla\alpha_l}{|\nabla\alpha_l|} \tag{12}$$

2.4. Numeircal Details

The generic CFD code ANSYS CFX11 was utilized as the simulation platform. The governing equations were discretized by the finite volume approach. The convection terms were approximated by a high order resolution scheme:

$$\phi_i = \phi_u + \xi\nabla\phi\cdot\Delta\boldsymbol{r} \tag{13}$$

where ϕ_u is the upwind vertex value and $\boldsymbol{r}$ is the vector from the upwind vertex to the integration point. ξ is adjustable from 0 to 1 according to the flow condition [16]. In order to capture the cavity interface accurately, a compressive scheme which is antidiffusive by allowing ξ >1 was introduced to discretize the convection terms in the volume fraction equations. Details of the scheme can be found in reference [17]. The diffusion terms were approximated by the second-order central difference scheme while a second order scheme was used for the transient terms. To enhance the stability of the simulation, a direct coupled solver was adopted to solve the pressure and velocities in one coupled matrix. The fundamental basis of this coupled solver derives from the significant development of Rhie and Chow [18] where they have proposed a formulation by expressing the pressure in terms of its neighbouring velocity values. Then the volume fractions are solved seperately.

3. MODEL VALIDATION

The numerical model was validated against the experiments carried out at St. Anthony Falls Laboratory of the University of Minnesota [11] which focused on the ventilated cavity with low Froude number. Three dimensionless parameters including the Froude number Fr, the ventilation rate $\overline{Q_g}$ and the cavitation number σ_c are adopted to decribe the working condition:

$$Fr = \frac{u_\infty}{\sqrt{gD_n}}, \overline{Q_g} = \frac{\dot{Q}_g}{u_\infty D_n^2}, \sigma_c = \frac{p_\infty - p_c}{0.5\rho_l u_\infty^2} \tag{14}$$

As shown in Figure 1, good agreement was observed between the predicted cavity shape and the experimental photos under different ventilation rate, confirming the accuracy of the numerical model for capturing the large scale gas-liquid interface.

4. RESULTS

4.1. Evolution of Ventilated Cavity with High Froude Number

Aiming at investigating the evolution process of ventilated cavity with high Froude number where the interactions between three phases of vapor, liquid and ventilated-gas should be considered, the numerical model was applied for a 1.2 m length underwater vehicle with Φ30 mm cavitator installed in the front. Figure 2 presents the development of the transient cavity shape at various ventilation rate when the cavitating body sailed at a high speed of 70 m/s. Before the startup of the ventilation process (t = 0), natural partial cavities were observed at the front and the tail of the cavitating body, called the primary and secondary cavity respectively. As the non-condensible gas injected into the natural cavity, the liquid evaporation rate was decreased, leading to the shrinkage of the vapor phase. When the ventilation rate was not high enough to expand the cavity size, e.g. $\overline{Q_g}$=1, the primary cavity size remained the same as the original natural cavity. As the ventilation rate increased ($\overline{Q_g}$=2), the cavity pressure was raised dramatically, resulting in the disappearance of the vapor phase at t = 0.15 s. Thereafter, the cavity gradually expanded and a supercavity with irregular vortex shedding off at the cavity tail was formed at t = 0.25 s. When the ventilation rate was further doubled ($\overline{Q_g}$=4), the cavity size increased significantly ever since the injection of the non-condensible gas, causing a supercavity generated at t = 0.15 s. Subsequently, due to the gravity effect, the cavity tail was gradually floated up, giving rise to the formation of twin-vortex tubes at the cavity tail. Hereafter, the expanding speed of the cavity declined fast with the elevated gas-leakage rate which will finally balance the ventilation rate to stabilize the cavity. In summary, the evolution processes of the ventilated cavity with high Froude number which grew from partial cavity to supercavity, undergoing different gas-leakage mechanisms were successfully captured by the numerical model.

4.2. Hydrodynamics Analysis for the Cavitating Body

In order to better understand the drag reduction mechanisms for the cavitating body, the hydrodynamics analysis was performed for the cavitating body. Figure 3 presents the steady cavity shape under different cavitation rate for the low Froude number Cases (Fr =18) which was resulted from low sailing speed. Owing to the gravity effect, remarkable asymmetry was observed for the cavitating body. Part of the lower body surface was exposed to the liquid while most of the ventilated gas was leaked through the twin-vortex tubes above the upper surface. Even when the ventilation rate was doubled, the lower surface area covered by the cavity was only slightly increased. This was

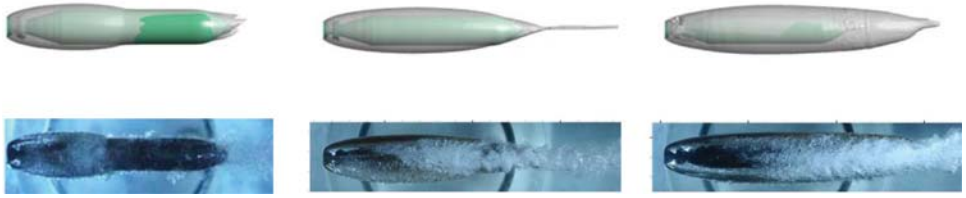

(a) $\overline{Q}_g = 0.08, \sigma_c = 0.25$ (b) $\overline{Q}_g = 0.12, \sigma_c = 0.15$ (c) $\overline{Q}_g = 03, \sigma_c = 0.11$

Figure 1. Comparison of the predicted cavity shape with the experimental photos [11].

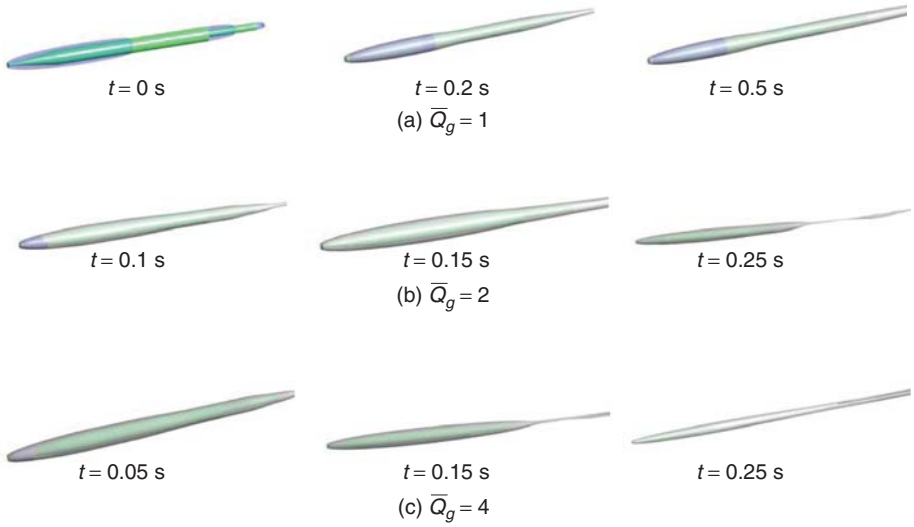

Figure 2. Evolution process of the ventilated cavity at various ventilation rate (The liquid volume fraction isosurface at 0.5 is represented by the grey semitransparent surface, and the vapor volume fraction isosurface at 0.5 is displayed by the blue semitransparent surface).

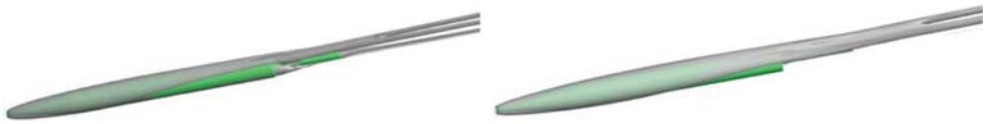

Figure 3. Predicted cavity shape for the cavitating vehicle with low Froude number.

mainly attributed by the widen of the twin-vortex tubes, which lead to the quick leakage of the additional ventilated gas. It is concluded that it is hard to form a supercavity covering the overall body when the vehicle sails at a low speed which will induce lift force for the cavitating body.

Figure 4 displays the hydrodynamics variation along with the ventilation rate for the cavitating body with low Froude number, where C_f, C_p and C_d refer to the friction drag coefficient, pressure drag coefficient and total drag coefficient respectively. C_l is the lift coefficient for the cavitating body. The friction drag was found descending dramatically in the case of low ventilation rate. When the cavity transited into gas-leakage by twin-vortex tubes, the friction drag dropped moderately due to the low expanding speed of the ventilated cavity. The variation of the total drag tightly follows the pressure drag curve which is characterized by a single-bottom distribution, indicating the dominant effect of pressure drag acting on the total drag. In the case of low ventilation rate, the wet area in the cone section which was partially covered by the cavity was decreased as the expanding of the cavity size, resulting in the reduction of the shoulder pressure drag. When the cone section was totally covered by the cavity, the increased cavity pressure induced higher pressure at the cone section, contributing to the ascending of the pressure drag. On the contrary, the lift curve presents a single-peaked distribution. At the initial ventilation stage, the asymmetry of the cavity shape was enhanced as the increasing of the ventilation rate, bringing on the ascending of the lift force until the peak point. Whereafter, the lift coefficient was observed gradually dropping, mainly caused by the weakened pressure difference between the upper and lower body surface as the cavity extending to cover larger area on the lower side. In general, the controllability as well as the overall performance for the cavitating vehicle with low Froude number is optimized when the ventilated cavity closes on the cone-cylinder intersection point, presenting the lowest pressure drag coefficient and highest lift coefficient.

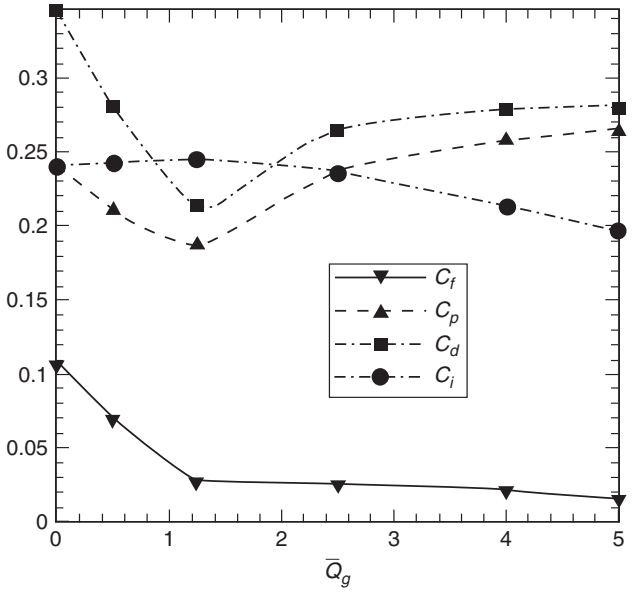

Figure 4. Hydrodynamics coefficents for the cavitating body with low Froude number.

(a) $\bar{Q_g} = 1.25$, $\sigma_c = 0.036$ (b) $\bar{Q_g} = 2.5$, $\sigma_c = 0.022$

Figure 5. Predicted cavity shape for the cavitating vehicle with high Froude number.

Figure 5 displays the predicted cavity shape for the cavitating body with high Froude number which was found less affected by the gravity effect than that in Figure 3. Along with the increasing of the ventilation rate, the ventilated cavity transited from a partial cavity to a supercavity ending with twin-vortex tubes. Considering the dominant effect of the pressure drag on the total drag, the variation of pressure drag coefficient along with the ventilation rate is given in Figure 6 where similar variation trend is observed as that in Figure 4. However, natural cavity covering the cone section was formed without ventilation in the case of high Froude number. The drag reduction at the initial stage was induced by the rise of the cavity pressure at the body tail. The initial pressure drag was greatly reduced for the higher Froude number case in Figure 6 because a larger natural cavity was generated without ventilation. An optimum ventilation rate is also observed for the ventilated cavitating body with high Froude number to minimize the drag coefficient.

4.3. A Universal Gas-Leakage Model for Ventilated Supercavity

Based on the numerical simulation, the variation of cavitation number along with the ventilation rate was obtained as shown in Figure 7. The result calculated by Epshtein's formula [19] for low Froude number condition was given as well, aiming at comparing the curves resulted from different gas-leakage mechanisms. The variation curve for the low Froude number (Fr =18), resulted from the twin-vortex tube gas-leakage scheme, is characterized by the sharp rising of the gas-leakage rate with the cavitation number decreasing and the minimum cavitation number. When the Froude number is increased (Fr =54), the ventilated cavity experiences transition between different gas-leakage methods. In the high cavitation number region where the re-entrained jet gas-leakage mechanism dominates, the gas-leakage rate increases slowly along with the decreasing of cavitation number. As the cavitation number reduced under the transition point, the gas-leakage rate varies in accordance with the twin-vortex tube mechanism. However, the curve is shifted left due to the decrease of the minimum cavitaiton number in comparison with

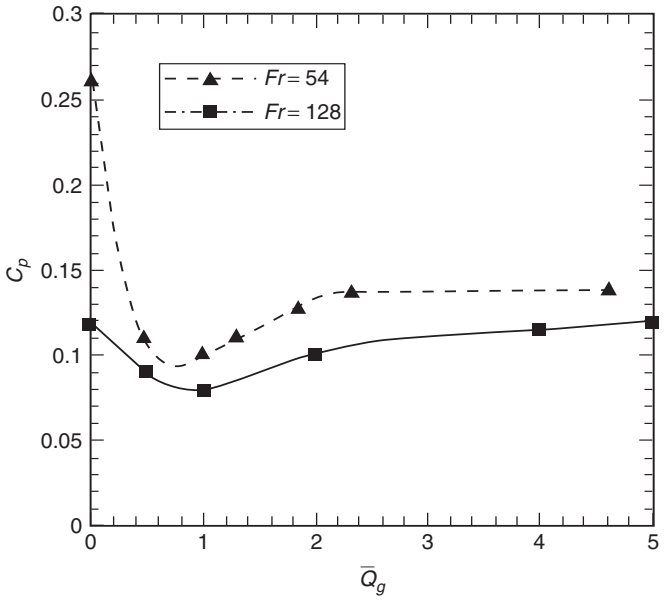

Figure 6. The variation of pressure drag factor along with ventilation rate.

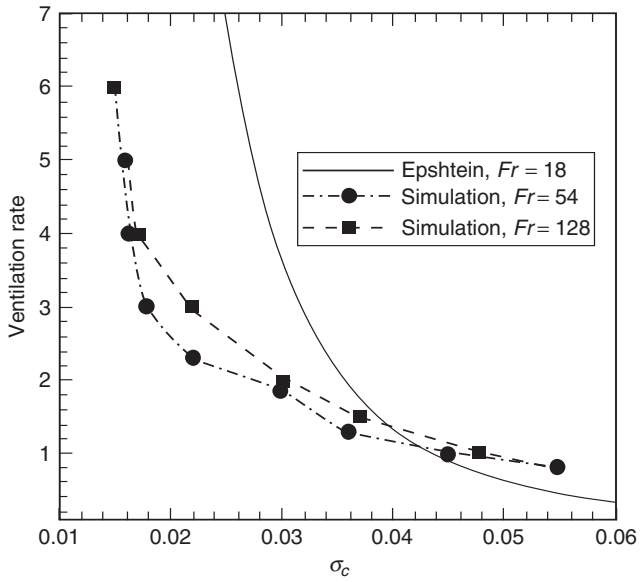

Figure 7. The variation of gas-leakage rate along with cavitation number under different Froude number.

the case of low Froude number. When the Froude number is further increased (Fr =128), the ventilated cavity only ends with re-entrained jet. In view of the tremendous effect the Froude number acting on the cavity shape, it is necessary to establish a universal gas-leakage model to consider different gas-leakage schemes.

In this paper, the gas-leakage rate was assumed to be determined by the dominant gas-leakage mechanism. The larger value between the gas-leakage rate caused by re-entrained jet $\overline{Q}_{g,r}$ and caused by twin-vortex tubes $\overline{Q}_{g,v}$ was adopted as the final gas-leakage rate.

$$\overline{Q} = \max(\overline{Q}_{g,r}, \overline{Q}_{g,v}) \tag{15}$$

The gas-leakage model by re-entrained jet was firstly established based on Spurk's [10] model which assumed the gas was leaked through the cavity boundary. As a matter of fact, when the cavitation

number is near the transition cavitation number which is affected by the Froude number, part of the gas in the cavity boundary layer is re-entrained into the cavity, causing a low probability of gas-leakage by re-trained jet. Therefore, Spurk's [10] model is improved using a re-entrained factor *I*:

$$\overline{Q}_{g,r} = Ik\frac{(1+\sigma_c)}{\sigma_c}\sqrt{\frac{1}{\sigma_c}\mathrm{In}\frac{1}{\sigma_c}} \tag{16}$$

The re-entrained factor is defined as:

$$I = 1-\exp\left\{-0.46\left[\frac{\sigma_c-\sigma_{c,\min}}{a(\sigma_{crit}-\sigma_{c,\min})}\right]^3\right\} \tag{17}$$

where a is adopted to adjust the range of the transition region. The transition cavitation number σ_{crit} and minimum cavitation number $\sigma_{c,\,\min}$ are calculated as [3]:

$$\sigma_{crit} = 1/Fr, \sigma_{c,\min} = 1.27(C_{D,0}Fr^{-4})^{1/3} \tag{18}$$

Epshtein's model for the ventilated cavity with twin-vortex tubes is adapted to taking into account wide range of Froude number:

$$\overline{Q}_{g,v} = \frac{0.42c_{x0}^2}{(\sigma_c-\Delta\sigma)[(\sigma_c-\Delta\sigma)^3 Fr_{ref}{}^4 - 2.5c_{x0}]}, Fr_{ref} = 4\sim 20 \tag{19}$$

where Fr_{ref} is the referenced Froude number. The translation value $\Delta\sigma$ is calculated as:

$$\Delta\sigma = 0.8(\sigma_{c,\min}-\sigma_{c,ref}) \tag{20}$$

where $\sigma_{c,\,ref}$ is the minimum cavitation number corresponding to the referenced Froude number. According to the simulation result, the natural cavitation number should be taken as the minimum value of the ventilated cavitation number.

In application of the proposed model, the variation of the gas-leakage rate with the cavitation number for the low Froude number condition was obtained as shown in Figure 8 where reasonably

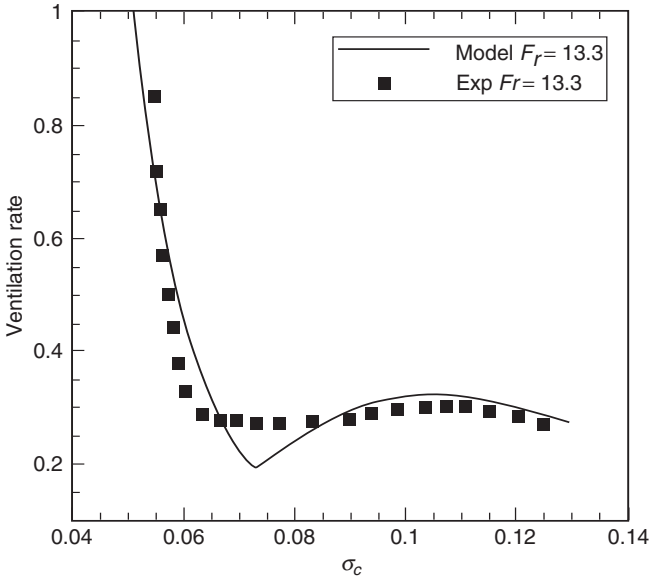

Figure 8. Comparison between calculated gas-leakage rate with the experimental data [20] for low Froude number condition.

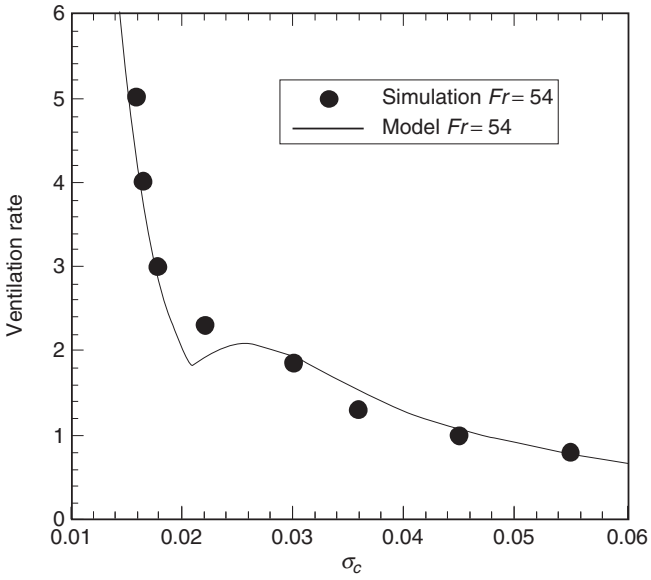

(a) $Fr = 54$

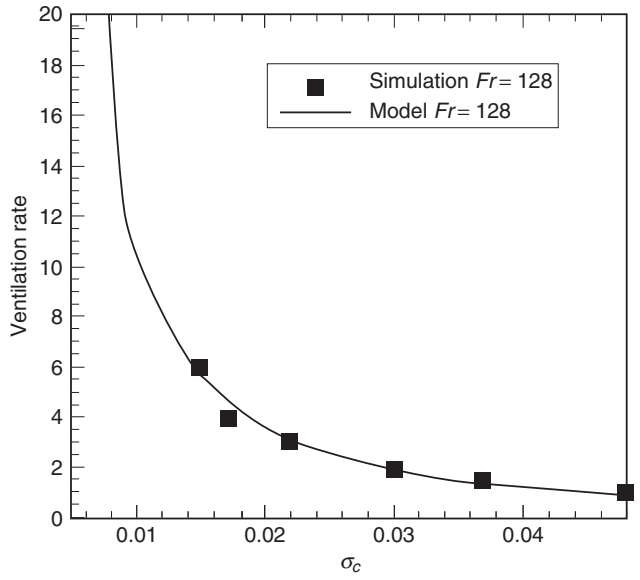

(b) $Fr = 128$

Figure 9. Comparison between calculated gas-leakage rate with the simulation results for high Froude number condition.

good agreement is observed in comparison against the experimental data. However, discrepancy is observed in the transition region due to the unstable gas-leakage in this stage. Figure 9 compares the calculated result for the ventilated cavity with high Froude number against the simulation result. Good coincidence is observed, indicating the effective of the proposed model.

5. CONCLUSIONS

The three-dimensional simulation model for the ventilated cavitating flow which considers interaction between three phases including vapor, ventilated gas and liquid was established based on the homogeneous multiphase model. Transient development processes were obtained for the ventilated cavity with high Froude number which undergone transition between different gas-leakage schemes. A minimum ventilation rate is required to expand the ventilated cavity larger than the initial natural cavity by replacing the vapor phase with the ventilated gas. Hydrodynamics

analysis was carried out for the cavitating body with wide range of Froude number. In the case of low Froude number, highly asymmetrical cavity induced by the great gravity effect will generate lift force for the cavitating body. An optimum ventilation rate exists to get the lowest pressure drag coefficient and highest lift coefficient. In the case of high Froude number, an optimum ventilation rate is also observed to minimize the pressure drag. Based on the simulation results, the variation of cavitation number along with the ventilation rate was obtained. A universal gas-leakage model which was adapted to a wide range of Froude number and various gas-leakage mechanisms was proposed for the ventilated supercavity. The model was validated in comparison with experimental and simulation results. The conclusions in this paper provides valuable method in assisting the design for the ventilated cavitating vehicle.

ACKNOWLEDGMENT

The financial support provided by the National Natural Science Foundation of China (NSFC 51176101) is gratefully acknowledged.

REFERENCES

[1] Savchenko Y N. Investigation of high-speed supercavitating underwater motion of bodies[R]. High-speed motion in water AGARD Report, 1998.

[2] Schauer T J. An experimental study of a ventilated supercavitating vehicle[D]. MS Thesis in Aerospace Engineering, University of Minnesota, 2003.

[3] Semenenko V N. Artificial Supercavitation. Physics and Calculation[C]. VKI Special Course on Supercavitating Flows., Brussels, Belgium, 2001.

[4] Stinebring D R, Cook R B, Dzielski J E, et al. High-speed supercavitating vehicles[C]. AIAA Guidance, Navigation, and Control Conference and Exhibit, Keystone, Colorado, 2006.

[5] Ceccio S L. Friction drag reduction of external flows with bubble and gas injection[J]. Annu. Rev. Fluid Mech, 2010(42): 183–203.

[6] Self M W, Ripken J F. Steady-state cavity studies in a free-jet water tunnel[R]. St. Anthony Falls Hydraulic Laboratory, University of Minnesota, 1955.

[7] Waid R L. Cavity shapes for circular disks at angles of attack[R]. California Institute of Technology, 1957.

[8] Campbell I J, Hilborne D V. Air entrainment behind artificially inflated cavities[C]. Second Symposium on Cavitation on Naval Hydrodynamics, Washington, 1958.

[9] Cox R N, Clayden W A. Air entrainment at the rear of a steady cavity[C]. Proceedings of the N.P.L. Symposium on Cavitation in Hydrodynamics, London, 1956.

[10] Spurk J H. On the gas loss from ventilated supercavities[J]. Acta Mechanica, 2002: 125–135.

[11] Schauer T J. An experimental study of a ventilated supercavitating vehicle[D]. MS Thesis in Aerospace Engineering, University of Minnesota, 2003.

[12] Launder B, Salding D. Lectures in Mathematical Models for turbulence[M]. Academic Press, 1972.

[13] Singhal A K, Li H. Mathematical basis and validation of the full cavitation model[J]. Journal of Fluids Engineering, 2002, 124: 617–624.

[14] Ansys. CFX-11 User Manual. ANSYS CFX[J]. 2007.

[15] Brackbill J U. A continuum method for modeling surface tension[J]. Journal of Computational Physics, 1992, 100(2): 741–750.

[16] Barth T J, Jesperson D C. The design and application of upwind schemes on unstructured meshes[C]. 1989.

[17] Zwart P J. Numerical modelling of free surface and cavitating flows[C]. VKI Lecture Series: Industrial Two-Phase Flow CFD, 2005.

[18] Rhie C M, Chow W L. Numerical study of the turbulent-flow past an airfoil with trailing edge separation[J]. AIAA Journal, 1983, 21(1525–1532).

[19] Epshtein L A. Methods of theory of dimensionality and similarity in problems of ship hydromechanics[M]. Leningrad: Sudostroenie Publishing House, 1970.

[20] Semenenko V N. Artificial Supercavitation. Physics and Calculation[C]. VKI Special Course on Supercavitating Flows., Brussels: RTO-AVT and VKI, 2001.